Leaf day respiration involves multiple carbon sources and depends on previous dark metabolism

Cyril Abadie, Julie Lalande, Corentin Dourmap, Anis Limami, Guillaume Tcherkez

Received: 6 October 2023 | Revised: 6 February 2024 | Accepted: 20 February 2024

DOI: 10.1111/pce.14871

ORIGINAL ARTICLE

Plant, Cell & Environment WILEY

Leaf day respiration involves multiple carbon sources and depends on previous dark metabolism

Cyril Abadie[1,2] | Julie Lalande[1] | Corentin Dourmap[1] | Anis M. Limami[1] | Guillaume Tcherkez[1,3]

[1]Institut de recherche en horticulture et semences, INRAe, Université d'Angers, Beaucouzé, France

[2]Ecophysiologie et génomique fonctionnelle de la vigne, Institut des Sciences de la Vigne et du Vin, INRAe, Université de Bordeaux, Villenave-d'Ornon, France

[3]Research School of Biology, ANU College of Science, Australian National University, Canberra, Australia

Correspondence
Guillaume Tcherkez, Institut de recherche en horticulture et semences, INRAe, Université d'Angers, 42 rue Georges Morel, 49070 Beaucouzé, France.
Email: guillaume.tcherkez@anu.edu.au

Funding information
Angers Loire Métropole; Conseil Régional des Pays de la Loire

Abstract

Day respiration (R_d) is the metabolic, nonphotorespiratory process by which illuminated leaves liberate CO_2 during photosynthesis. R_d is used routinely in photosynthetic models and is thus critical for calculations. However, metabolic details associated with R_d are poorly known, and this can be problematic to predict how R_d changes with environmental conditions and relates to night respiration. It is often assumed that day respiratory CO_2 release just reflects 'ordinary' catabolism (glycolysis and Krebs 'cycle'). Here, we carried out a pulse-chase experiment, whereby a $^{13}CO_2$ pulse in the light was followed by a chase period in darkness and then in the light. We took advantage of nontargeted, isotope-assisted metabolomics to determine non-'ordinary' metabolism, detect carbon remobilisation and compare light and dark ^{13}C utilisation. We found that several concurrent metabolic pathways ('ordinary' catabolism, oxidative pentose phosphates pathway, amino acid production, nucleotide biosynthesis and secondary metabolism) took place in the light and participated in net CO_2 efflux associated with day respiration. Flux reconstruction from metabolomics leads to an underestimation of R_d, further suggesting the contribution of a variety of CO_2-evolving processes. Also, the cornerstone of the Krebs 'cycle', citrate, is synthetised de novo from photosynthates mostly in darkness, and remobilised or synthesised from stored material in the light. Collectively, our data provides direct evidence that leaf day respiration (i) involves several CO_2-producing reactions and (ii) is fed by different carbon sources, including stored carbon disconnected from current photosynthates.

KEYWORDS

isotopic labelling, metabolic fluxes, metabolomics, photosynthesis

1 | INTRODUCTION

Illuminated leaves simultaneously assimilate CO_2 via gross photosynthesis (carboxylation) and liberate CO_2 via photorespiration and day respiration (the rate of which is denoted as R_d). Unlike carboxylation and photorespiration that can be modelled via Rubisco kinetics and thus CO_2 and O_2 mole fraction, day respiration is still insufficiently understood to build a model predicting CO_2 production rate as a function of environmental parameters (Huntingford et al., 2017; O'Leary et al., 2019). For example, steady-state modelling (Buckley & Adams, 2011) or temperature relationships between dark and day respiration (Gong et al., 2017) have been used to estimate R_d. However, no model like those used for photosynthesis has been proposed so far, simply because key metabolic events responsible for day respiratory CO_2 generation have not been identified with precision yet.

The lack of knowledge about day respiration could be problematic for computations of photosynthesis and CO_2 emission at the regional or global scale since it is a required parameter (Atkin et al., 2014). A conventional day respiration rate is commonly used (for a specific discussion, see Atkin et al., 2017). Also, R_d is required to compute internal conductance from leaf exchange and fluorescence, interpret $^{12}C/^{13}C$ isotope fractionation by net photosynthesis (Δ) or compute water use efficiency therefrom. For example, the model describing Δ originally assumes that day respiration is fed by current photosynthesis, with a fixed isotope fractionation (*e*) (Farquhar et al., 1989). However, there is experimental evidence suggesting that day respiration is also fed by reserves (stored carbon), and therefore an additional mathematical term is required to describe Δ (Tcherkez et al., 2011; Wingate et al., 2007). Quite critically, this term has net assimilation (*A*) and not carboxylation (v_c) in the denominator of the respiratory term (eR_d/A), and as a result, diverges to infinity at low photosynthesis (typically near the compensation point), leading to very high observed Δ values (Barbour et al., 2017). Although the contribution of stored, photosynthetically disconnected carbon to sustain day respiration is thus recognised, consequences for routine gas exchange and isotope fractionation are difficult to quantify or anticipate (particularly when environmental conditions vary) because metabolic fluxes, key substrates and their natural isotope composition are not well known.

In the past decades, intense efforts have been devoted to adding new measurements of R_d using several methods (Laisk, Kok, Yin or Gong methods, e.g., see Tcherkez et al., 2017, for a review). Day respiration (CO_2 production rate in the light) is often found to be lower (between 0.5 and 1 μmol m^{-2} s^{-1} in many cases) than the dark respiration rate (1–2 μmol m^{-2} s^{-1}), suggesting that some CO_2-generating metabolic steps are inhibited in the light compared to the dark (Atkin et al., 1997, 2015; Heskel et al., 2013). Accordingly, advances have been made to describe how the two canonical decarboxylation steps of catabolism (pyruvate dehydrogenase, and the tricarboxylic acid pathway (TCAP) also referred to as Krebs 'cycle') are regulated in the light (for a review, see Tcherkez, Boex-Fontvieille, et al., 2012). In particular, mitochondrial pyruvate dehydrogenase (PDH) is down-regulated by phosphorylation in the light (Budde & Randall, 1990; Gemel & Randall, 1992), and TCAP enzyme activities are partly inhibited or slowed down (Gessler et al., 2017; Hanning & Heldt, 1993; Scheible et al., 2000; Tcherkez et al., 2009). The use of transgenics and inhibitors has also suggested that several enzymatic steps of the TCAP exert a control on the carbon flux, in particular CO_2-evolving 2-oxoglutarate dehydrogenase (Araújo et al., 2008; Araújo et al., 2012), suggesting that this step may be effectively restricted in the illuminated leaf. The synthesis of carbon backbones required by nitrogen assimilation involves reserve remobilisation and it has been shown using isotopic tracing in the light (with $^{13}CO_2$ or ^{13}C subtrates) that citrate production is enhanced in the dark compared to the light (Tcherkez et al., 2008; Tcherkez, Mahe, et al., 2012). Also, pioneering experiments with $^{14}CO_2$ have shown modest radioactivity in citrate in the light, that could be increased using a period of darkness after ^{14}C-labelling (Graham & Walker, 1962). Accordingly, analysis of metabolic diel cycles has shown that the leaf citrate pool increases during the night and decreases during the day, suggesting nocturnal citrate accumulation via the TCAP and citrate utilisation during the night (Flis et al., 2019; Scheible et al., 2000). Using nuclear magnetic resonance (NMR) analysis, it has been suggested that Ala, Asp and Glu synthesised in the light partly originate from stored carbon, showing indeed that the influx of photosynthetic carbon into catabolism (pyruvate, oxaloacetate [OAA] and 2-oxoglutarate synthesis) is modest in the light (Abadie, Lothier, et al., 2017). However, it should be recognised that the sum of rates associated with PDH and TCAP decarboxylation is generally lower than observed R_d. For example, in cocklebur and sunflower under standard conditions (21% O_2, 380 μmol mol^{-1} CO_2, 21°C), PDH- and TCAP-mediated decarboxylation account for about 0.3 μmol m^{-2} s^{-1} (including when isotopic dilution is accounted for in labelling experiments) (Tcherkez et al., 2005; Tcherkez et al., 2008). In other words, some proportion of observed day respiratory CO_2 production is presently unexplained. Also, it must be remembered that observed R_d is a net flux, encompassing both CO_2 production by metabolism and CO_2 fixation via anaplerosis (phospho*enol*pyruvate carboxylase [PEPC]-catalysed fixation) (Abadie & Tcherkez, 2019a). It means that a significant proportion of 'gross' day respiratory CO_2 efflux comes from pathways other than PDH and TCAP reactions.

In our previous study, we used $^{13}CO_2$ labelling of sunflower leaves (*Helianthus annuus* L.) in the light under various CO_2/O_2 conditions (Abadie et al., 2021). Using nontargeted metabolomics, we found that carboxylation/oxygenation conditions impacted on several metabolic pathways that could affect day respiration, such as branched-chain amino acids. However, differences with dark respiration were ignored and furthermore, the potential contribution of reserves (and thus delayed utilisation of ^{13}C atoms) could not be monitored. To solve this problem, we applied principles of pulse-chase experiments (Bacher et al., 2016; Dieuaide-Noubhani et al., 2007) whereby after a $^{13}CO_2$ labelling period in the light, leaves were kept in the dark and then illuminated under an atmosphere with CO_2 at natural ^{13}C abundance (for an example of

pulse-chase experiment with *Arabidopsis*, see Huege et al., 2007). We used the same species, sunflower, so as to take advantage of our previous results, in particular in calculations. We did a nontargeted analysis of metabolic features to follow isotopologues (^{12}C, $^{13}C_1$, $^{13}C_2$, etc., species) separately and thus could appreciate concurrent changes in total pool size and turnover (the differential behaviour of isotopologues depending on pool size and turn-over rate is illustrated in Supporting Information: Figures S1 and S2). Our data are broadly consistent with previous findings (citrate de novo synthesis more pronounced in the dark than in the light) and show that several noncanonical, metabolic pathways using either current photosynthetic carbon or stored carbon, participate in day respiratory CO_2 efflux.

2 | MATERIAL AND METHODS

2.1 | Plant material

Sunflower seeds (*Helianthus annuus*, var. XRQ) were sown in potting mix (Martins potting mix) and transferred to 15 L pots after 2 weeks. Plants were grown in the greenhouse under 24°C/18°C, 60%/55% relative humidity, 16/8 h photoperiod (day/night), with natural light supplemented by Lucagrow 400 W sodium lamps (JB Lighting). Plants were watered every 2 days supplemented once a week with 1.5 g L^{-1}nutrient solution Peters® Professional Pot Plant Special (Everris) with a $N/P_2O_5/K_2O$ composition of 15/11/29 (and a nitrogen balance nitrate/ammonium/urea of 8.6/2.0/4.4). Plants were used for experiments 50 days after sowing. We used leaves of rank 5–7, which are the mature source leaves with maximum photosynthetic capacity at this developmental stage.

2.2 | Gas exchange and sampling

The overall design of the experiment is depicted in Supporting Information: Figure S3. Plants used for gas exchange and labelling were taken from the glasshouse at a fixed time (4 h after the onset of light) so as to avoid potential diel cycle effects. Gas exchange and sampling were done as in (Abadie & Tcherkez, 2019a, 2019b) with an adapted chamber coupled to the LI-COR 6400-XT (LI-COR Biosciences). Gas-exchange conditions were: 380 µmol mol^{-1} CO_2, 400 µmol m^{-2} s^{-1} photosynthetically active radiation when in the light, 80% relative humidity, gas flow 35 L h^{-1}, and 21–23°C air temperature. Day respiration (R_d) was estimated using the Laisk method (Laisk & Loreto, 1996) using three light intensities (250, 500 and 800 µmol m^{-2} s^{-1}) and four CO_2 mole fractions in the region of photosynthetic linear response (C_a at 5, 40, 80 and 120 µmol mol^{-1}, i.e., C_i of about 15, 40, 70 and 100 µmol mol^{-1}). Isotopic labelling was performed using $^{13}CO_2$ (Sigma-Aldrich; 99% ^{13}C) for 2 h after 40 min to 1 h of photosynthetic induction to reach the photosynthetic steady state. After 2 h under $^{13}CO_2$, the light was switched off and inlet CO_2 was changed to ordinary CO_2 (natural ^{13}C abundance). After 2 h, the light was switched on again, with ordinary CO_2 in inlet air. We did sampling (i.e., a leaf was killed) at the end of each step: just after 2 h in the light under $^{13}CO_2$ (pulse; referred to as 'Light' and coloured in yellow in figures), at the end of the dark period (chase in darkness; referred to as 'Light+Dark' and coloured in grey in figures), and at the end of the light period under ordinary CO_2 (chase in the light; referred to as 'Light+Dark+Light' and coloured in orange in figures). Identical experiments without labelling (only CO_2 at natural abundance throughout) were also carried out so as to have a background isotope signal: this was strictly necessary to check that metabolites were effectively at natural abundance (1.1%) and also to measure pool sizes (Gout et al., 1993).

2.3 | Extraction and NMR isotopic analyses

Samples were extracted with perchloric acid in liquid nitrogen as in Aubert et al. (1994). The perchloric extract was neutralised and freeze-dried. The freeze-dried extract was resuspended in 1.5 mL water (10% D_2O). 10 and 20 µL were collected for gas chromatography coupled to mass spectrometry (GC-MS) and liquid chromatography (LC)-MS, respectively. The GC-MS aliquot was frozen and spin-dried. ^{13}C-NMR analyses were performed as in Abadie & Tcherkez (2019a) at 298 K (25°C) without tube spinning, using an inverse-gated pulse programme (zgig) with 90° pulses for ^{13}C (10 µs). Acquisition parameters were: 0.89 s acquisition time, 65k size of free induction decay (FID), and a relaxation delay (D1) of 1.2 s (and dwelling time 200 µs). Twenty thousand scans were done, representing about 9 h analysis per sample. ^{13}C-signals were normalised to the internal standard (maleate).

2.4 | Untargeted metabolomics (LC-MS, GC-MS)

LC-MS analyses were carried out as in Abadie et al. (2021), using a LC-MS UHPLC/Orbitrap® (Dionex/Thermo Fisher Scientific) coupling, from the 20-µL aliquot (see above) diluted 10 times in ultrapure water, with trifluoromethyl phenylalanine (TFP) as an internal standard. For metabolites considered here, external calibration curves (with TFP as an internal standard) were used for quantification of pool sizes. GC-MS analyses were carried out as in Abadie, Blanchet et al. (2017), using GC-MS, via methanol:water extraction of the spin-dried aliquot followed by derivatization with methoxylamine and N-methyl-N-(trimethylsilyl) trifluoroacetamide in pyridine. Alkanes were used in each sample to compute the retention index. Signals were normalised by the internal standard (ribitol).

2.5 | Data extraction

Nontargeted analysis was conducted to extract 'features' from metabolomics analyses. The term 'features' refers to an individual metabolic quantitative variable. In NMR, LC-MS and GC-MS a feature

is a ^{13}C-signal referred to by its chemical shift, an m/z ion + retention time couple, and an m/z ion + retention index couple, respectively. Nontargeted analysis was carried out as in Abadie et al. (2021) using TopSpin 4.1.4 (direct export of spectral data; decomposition of the spectrum in 1-ppm wide buckets), Metabolome Express and MzMine2 for NMR, GC-MS and LC-MS, respectively.

2.6 | Statistics

Considering the number of metabolic features to be handled (in particular with GC-MS and LC-MS), it was useful to carry out both multivariate analyses in addition to classical univariate analyses (analysis of variance [ANOVA]). Here, we opted for a two-factor analysis, whereby we have the effect of isotopic substitution (^{13}C labelling vs. natural abundance), the effect of 'conditions' (Light, Light + Dark, Light + Dark + Light) and their interaction. Quite obviously, the most interesting effect here was the interaction effect, because it showed the impact of light and dark on isotopic enrichment and thus was instrumental to follow metabolic turnover. Multivariate statistics were carried out using orthogonal projection on latent structure (OPLS; with Simca®, Umetrics) using labelling and 'conditions' as qualitative Y variables, and metabolic features as predicting X variables. Before running the OPLS, a principal component analysis was conducted to check the presence of outliers (samples outside Hotelling's ellipse). The performance of the OPLS was assessed using the correlation coefficient between predicted and observed Y (R^2), the cross-validated correlation coefficient (Q^2), the Q^2 intercept of the permutation test (that was checked to be negative), and the p value of testing the OPLS model against a random-error model (i.e., average±error) via a χ^2 test (this p value is referred to as $P_{CV\text{-}ANOVA}$) (Bylesjö et al., 2006; Eriksson et al., 2008). The performance of OPLS models is summarised in Supporting Information: Table S1. Univariate statistics were conducted with a two-way ANOVA, with labelling (^{13}C vs. natural abundance) and 'conditions' as factors. Statistical significance was considered when $p < 0.01$ when the number of features was modest (NMR, GC-MS) or using the Bonferroni threshold (implemented as in (Tan & Xu, 2014)) when the number of features was high and thus the false discovery probability had to be controlled (LC-MS). Univariate and multivariate analyses were combined using −log(P-value) (univariate) plotted against the OPLS loading (pq) in a 'volcano plot'. In such a representation, the best metabolic markers are at the extremity of the plot (upper left and upper right). In volcano plots, different colours were used to differentiate features associated and not associated with an interaction (labelling × 'conditions') effect.

2.7 | Calculations

Fluxes associated with CO_2 fixation and CO_2 production were estimated using isotopic data. Only pathways where significant metabolites (features) were found in analyses were considered. The isotope composition (%^{13}C) of the metabolite of interest and its precursor were used to calculate the turn-over and thus the flux using the pool size. The number of times the pool was turned over (N) was estimated using a logarithm relationships as in (Schnyder et al., 2012):

$$N = -\ln\left(\frac{p_{prec} - p}{p_{prec} - p_o + \varepsilon t p^*}\right) - \varepsilon t, \quad (1)$$

where p and p_{prec} are the %^{13}C in the metabolite of interest and its precursor, respectively. p_o is ^{13}C natural percentage (1.1%). The flux through the pool of the metabolite of interest (µmol m^{-2} s^{-1}) was thus calculated as $f = N \times Q/t$ where Q is pool size (µmol m^{-2}) and t is the time of the phase of interest (here, 2 h, i.e., 7200 s). $\varepsilon t p^*$ and εt are correction factors accounting for the change in pool size, where ε is the relative change in pool size (in s^{-1}) and p^* is the average value of p_{prec} between 0 and t. The mathematical justification of Equation (1) is detailed in Supporting Information: Notes S1. Specific calculations were carried out for PEPC fixation and malic enzyme activity (see Supporting Information: Notes S2) since there is some cyclicity in malate and pyruvate metabolism and thus Equation (1) was not applicable.

3 | RESULTS

3.1 | Overview of ^{13}C labelling via NMR analysis

As expected, there was a general increase in the ^{13}C signal across the NMR spectrum, showing that carbon fixed by photosynthesis was used broadly by metabolic pathways. Most labelled metabolites were sugars (60–110 ppm region), with a considerable increase in ^{13}C signal (Figure 1a). An ANOVA analysis was conducted to find NMR features (buckets) associated with significant effects. Many features were associated with a labelling effect and 18 features were associated with a 'condition' effect such as sugar carbon atoms, and serine and glycine C-1 atoms (not shown). Seventeen features were associated with an interaction effect, and they are illustrated in Figure 1b with a hierarchical clustering. Three clusters were observed: C-atom positions particularly enriched during the pulse phase in the light and then showing substantial ^{13}C disappearance during the chase (C-4 of malate and C-1 of fructose) (cluster A); C-atoms positions strongly labelled in the light during the pulse and showing a slow decrease during the chase (mostly sucrose C-atoms) (cluster B); and C-atoms not labelled in the light but labelled only during the chase (C-1 of gentiobiose, C-2/4 of citrate and C-4 of glutamate) (cluster C). That is, gentiobiose, citrate and glutamate were not synthesised in the light from current photosynthates to a great extent. Rather, dark metabolism was necessary for their de novo synthesis using ^{13}C. Buckets associated with these three metabolites are shown in detail in Figure 1c–e. Unsurprisingly, citrate C-2/4 formed a broad peak (this is usual using ^{13}C-NMR due to chelation of citrate with cations) (Figure 1c). Glutamate (C-4 atom)

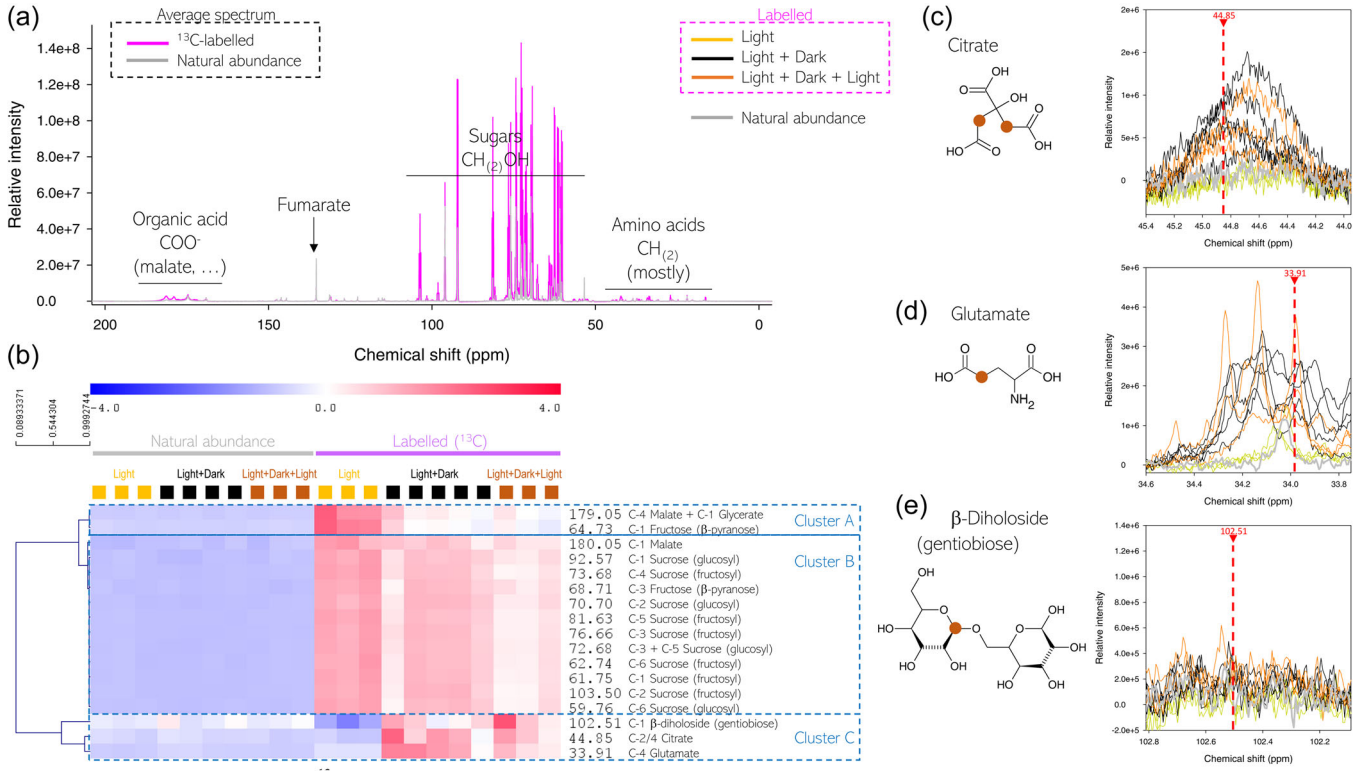

FIGURE 1 Significant metabolic features from ^{13}C-NMR analysis. (a) Overview of the full average spectrum showing the most important regions. (b) Heatmap with hierarchical clustering showing buckets (1 ppm width) associated with a significant labelling × conditions effect ($p < 0.01$, two-way ANOVA). On the right-hand side, the average chemical shift (in ppm) across the bucket of interest is shown. (c–e) Illustration of significant buckets of cluster C in (b), showing C-atom positions (orange dots) with chemical formulae. (b) The vertical dashed red line stands for the average chemical shift reported. (b, e) The NMR signal at 102.51 ppm corresponds to the C-1 atom of a β-(1 → 6)diholoside, and gentiobiose is given as an example. The C-1 atom of the β-conformer of erlose (gentianose; erlose is reported in Figure 2) would show the same chemical shift at C-1. ANOVA, analysis of variance; NMR, nuclear magnetic resonance.

was clearly more labelled in the dark (Light + Dark) and in the subsequent light phase (Light + Dark + Light), with peak multiplicity, showing the concurrent ^{13}C enrichment in neighbour C-atom positions (multiple ^{13}C labelling is addressed below with LC-MS) (Figure 1d). The signal in the C-1 atom of gentiobiose in the dark and during the subsequent light phase was above that in the light phase (or in natural abundance samples) but remained very low (Figure 1e). This was not surprising since gentiobiose is a minor sugar, far less concentrated than sucrose or glucose.

3.2 | ^{13}C-labelling in major compounds with GC-MS metabolomics

Metabolic features were analysed using GC-MS (nominal mass resolution) to check isotopic labelling in major compounds such as sugars, metabolites involved in photorespiration and abundant secondary metabolites. Features associated with a labelling effect are represented as a volcano plot in Figure 2a. Features more abundant with ^{13}C labelling comprised ^{13}C isotopologues of sucrose, raffinose and other sugars, along with isotopologues of photorespiratory intermediates (serine, glycerate) and secondary metabolites (caffeate, quinate) derived from erythrose 4-phosphate (Calvin cycle intermediate) and phospho*enol*pyruvate (PEP). Reciprocally, features more abundant without labelling were monoisotopic forms (i.e., ^{12}C species) of sucrose, photorespiratory intermediates and their derivative (glycerate, *N*-acetyl-serine), and secondary metabolites (salicylate, caffeate). There were relatively few metabolites significantly ($p < 0.01$) affected by 'conditions', only quinate appearing significantly more abundant in the dark (Figure 2b). Several sugar and sugar-related metabolites were more abundant in the light (monoisotopic forms of sucrose, glucuronate β-lactone, glucosamine, galactose, mannose 6-phosphate), as well as glycerate (both monoisotopic form and $^{13}C_2$ isotopologue) and glutamate.

Features associated with a significant interaction effect are shown as a heatmap in Figure 2c. Hierarchical clustering generated two groups (clusters A and B), mostly differentiating metabolites with an increased pool size in the light without labelling (cluster A) and metabolites without such an increase (cluster B). However, there were contrasted patterns of variation regardless of clusters (circled numbers): metabolites that were ^{13}C-labelled in the light, as revealed by the disappearance of the ^{12}C (monoisotopic) form, such as gluconate (1 and 4); metabolites with a decreased pool size in the dark, such as galactitol (2); a metabolite lower in the Light + Dark +

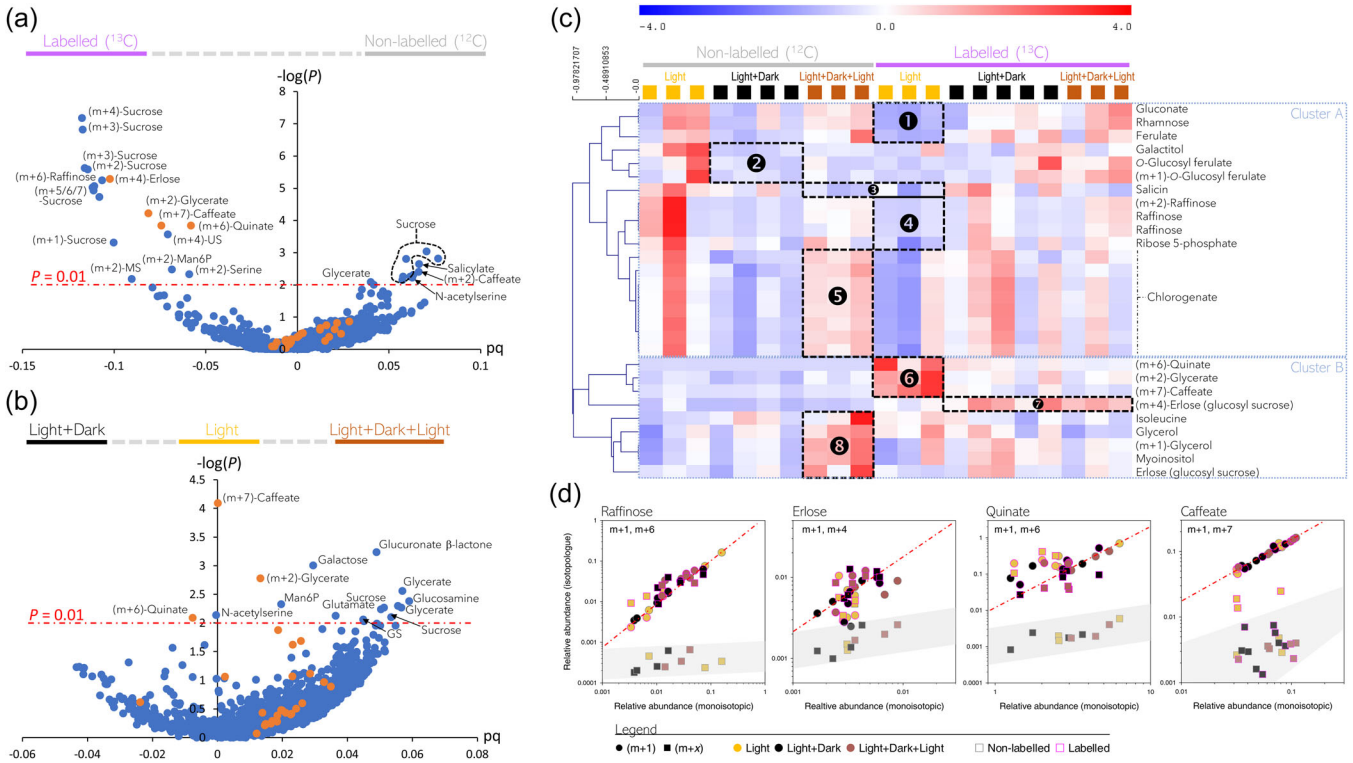

FIGURE 2 Significant metabolic features from GC-MS metabolomics. Volcano plots showing the best significant features associated with the effect of isotopic labelling (a) and light/dark conditions (b). The dashed red line stands for the threshold $p = 0.01$. Orange dots stand for features associated with an interaction effect. (c) Heatmap showing features significant for the interaction labelling × conditions effect, with hierarchical clustering (Pearson correlation) on the left. Numbers refer to specific situations discussed in the main text. (d) Relationship between monoisotopic *m/z* ions and isotopologues in selected metabolites, showing how multilabelled isotopologues are of minor importance at natural abundance area (grey shading) or are of greater importance, getting close to the monolabelled isotopologues. The red dashed line stands for the observed relationship between monoisotopic and monolabelled molecular species. Note the specific case of caffeate, where the multilabelled species is above natural abundance only after illumination with $^{13}CO_2$. GC-MS, gas chromatography coupled to mass spectrometry. [Color figure can be viewed at wileyonlinelibrary.com]

Light condition without labelling and in the light with labelling, i.e., with concurrent change in pool size and ^{13}C enrichment (salicin, 3); metabolites with a larger pool size in the light such a chlorogenate, glycerol and myoinositol (5 and 8); metabolites labelled (^{13}C isotopologues) in the light such as quinate, glycerate and caffeate (6) and erlose, a metabolite labelled only during the chase periods (Light + Dark and Light + Dark + Light) (7). The specific pattern of erlose is consistent with that of gentiobiose (Figure 1) and their synthesis probably originated from sugar interconversions during starch and fructan metabolism in the dark (Versluys et al., 2018).

To monitor isotopic species (isotopologues) of the carbon source for primary and secondary metabolism, a specific focus on significant isotopologues of raffinose, erlose, quinate and caffeate is provided in Figure 2d. The $^{13}C_1$ isotopologue of raffinose was always correlated to the ^{12}C (monoisotopic) form regardless of labelling, showing that both ^{12}C and $^{13}C_1$ forms reflected pool size (i.e., the $^{13}C_1$ isotopologue was more influenced by the pool size than labelling, see Supporting Information: Figures S1 and S2 for the theory, case no. 1 in Supporting Information: Figure S2). By contrast, the $^{13}C_6$ isotopologue abundance increased only upon labelling (pink-bordered squares). The same applied to erlose ($^{13}C_4$) and quinate ($^{13}C_6$). In the case of caffeate, this effect was also visible (but less pronounced) with the $^{13}C_7$ isotopologue. This simply shows that in these metabolites, ^{13}C labelling led to an increase in multisubstituted species, which were proportionally more impacted than the monosubstituted ($^{13}C_1$) species. This is not very surprising considering the prevalence of the multisubstituted ($^{13}C_3$) isotopologue of triose phosphates in the light with $^{13}CO_2$ (see Figure 3 below), which can be used as a carbon source for downstream metabolism.

3.3 | LC-MS metabolomics: Overview of significant features

Due to the number of features obtained by LC-MS analysis (13 864), there were many significant features even with the Benjamini–Hochberg correction of the probability threshold. In effect, 615 features were significantly affected by labelling (not shown), 99 were affected by 'conditions' (Supporting Information: Table S1,

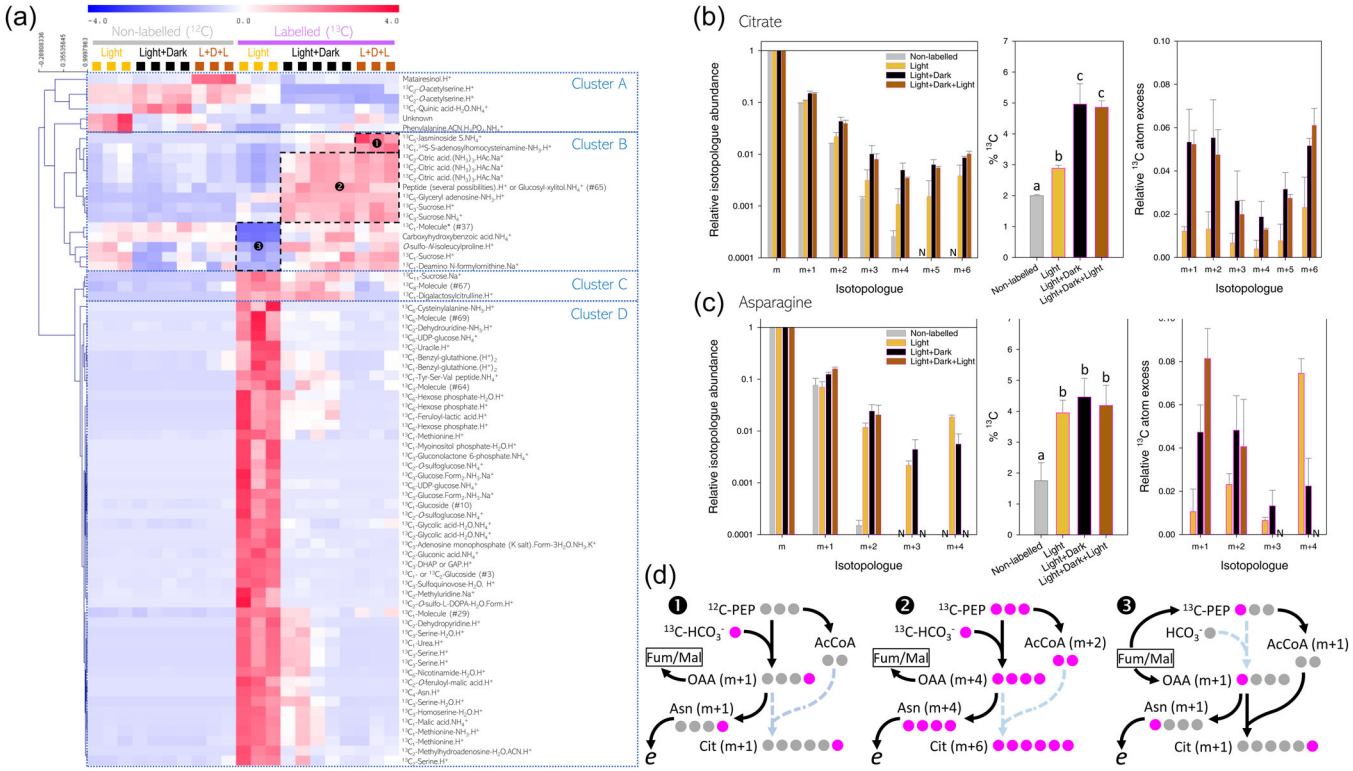

FIGURE 3 Significant metabolic features from LC-MS metabolomics. (a) Heatmap with hierarchical clustering showing features associated with a significant labelling × condition interaction effect (p value < Benjamini–Hochberg corrected threshold). (b and c) Focus on citrate and asparagine isotopologues, with the relative isotopologue abundance (relative to the monoisotopic species) in log scale, absolute %^{13}C and relative ^{13}C-atom excess (i.e., ^{13}C mole fraction above natural abundance). (d) Three scenarios illustrating the production of citrate and asparagine isotopologues: 1, situation in the light just after having turned to $^{13}CO_2$ (PEP not labelled yet), leading to monolabelled species; 2, situation in the light after some time under $^{13}CO_2$ (PEP is labelled), leading to multilabelled species and 3, situation in the dark, where some isotopologues (here illustrated with the monolabelled species) of remobilised C_4 acids lead to monolabelled asparagine and citrate. The randomisation via the TCAP is not shown for simplicity. Arrows in light blue stand for down-regulated steps. '*e*' stands for export and utilisation (protein synthesis) of asparagine. In (a), numbers with hash (#) aside names refer to feature numbering in Table 1, while circled numbers refer to specific groups discussed in the main text. Further information on other metabolites is provided in Supporting Information: Figure S6. (b and c) 'N' stands for 'not detected' and letters stand for statistical classes (p < 0.05, two-way ANOVA). AcCoA, acetyl-coenzyme A; Cit, citrate; LC-MS, liquid chromatography-mass spectrometry; OAA, oxaloacetate; PEP, phospho*enol*pyruvate; TCAP, tricarboxylic acid pathway. [Color figure can be viewed at wileyonlinelibrary.com]

illustrated as a volcano plot in Supporting Information: Figure S4) and 71 were affected by the interaction effect labelling × 'conditions' (Table 1, Figure 3a). Interaction-significant features formed four clusters: features more abundant under specific nonlabelling conditions, and less abundant under labelled conditions, such as the $^{13}C_2$ isotopologue of *O*-acetylserine and ^{12}C-phenylalanine (reflecting pool size and ^{13}C natural abundance; cluster A); features less abundant in the light upon labelling and more abundant during the chase (cluster B, described below); features (^{13}C isotopologues) increasing during the pulse and decreasing more (cluster D) or less (cluster C) rapidly during the chase. Clusters C and D comprised multisubstituted species of sugars (e.g., $^{13}C_{11}$-sucrose, $^{13}C_6$-hexose phosphates, $^{13}C_3$-triose phosphates) but also photorespiratory intermediates (e.g., $^{13}C_3$ isotopologue of serine), uracile-derived metabolites (e.g., $^{13}C_6$-UDP-glucose, $^{13}C_2$-uracile), organic acids ($^{13}C_1$-malate) and molecules of S metabolism (e.g., $^{13}C_1$-methionine, $^{13}C_3$-homoserine, $^{13}C_1$-benzylglutathione).

3.4 | Specific metabolites with a light/dark labelling pattern

Cluster B comprised citrate $^{13}C_2$ isotopologue, which had a low abundance in the light with $^{13}CO_2$ (pulse) and increased in the dark and in the light with $^{12}CO_2$ (chase). That is, de novo citrate synthesis from current photosynthates was low in the light and was much higher in the subsequent dark phase. Sucrose isotopologues with a small number of ^{13}C atoms ($^{13}C_3$) had a similar pattern, simply because the utilisation of nonlabelled triose phosphates from transitory starch remobilisation led to an isotopic dilution (in fact, $^{13}C_3$-triose phosphates nearly disappeared in the dark, see cluster D; see also Supporting Information: Figure S5 for their %^{13}C).

A specific focus on citrate isotopologues is provided in Figure 3b (where relative abundance is shown in the log scale). There was a general increase in ^{13}C isotopologues of citrate (not only $^{13}C_2$), in particular during the chase. As a result, the computed %^{13}C was

TABLE 1 List of LC-MS features associated with a significant interaction (isotope × condition) effect, that is, with a *p* value (two-way ANOVA) lower than the Benjamini–Hochberg corrected threshold.

Name	Possible identifications	Index MZMine	*m/z*	Retention time (min)	No.	*p* value
Sugars, glucosides and sugar derivatives						
$^{13}C_3$-DHAP or GAP.H^+	(triose phosphate)	4646	174.015340	5.91	1	0.00E+00
$^{13}C_3$-sulfoquinovose-$H_2O.H^+$		4952	230.033047	3.11	2	9.55E−15
$^{13}C_1$- or $^{13}C_2$-glucoside*	$^{13}C_1$-glucosyl-argininosuccinic acid.NH_4^+, or $^{13}C_1$-glucosyl-omphamurin (or other polyphenol $C_{16}H_{18}O_5$).NH_4^+, or $^{13}C_2$-glucosyl-dehydroartemisin.Na^+, or $^{13}C_2$-glucosyl-matricin/achillicin.H^+, or $^{13}C_2$-diglucosyl-hydroquinone.$NH_3.NH_4^+$	5995	471.209875	1.81	3	6.32E−14
$^{13}C_3$-Glucose.$Form_2$. $NH_3.Na^+$		5429	315.097321	7.55	9	9.46E−09
$^{13}C_1$-Glucoside*	$^{13}C_1$-*cis*-zeatinglucoside.H^+, or $^{13}C_1$-pantothenic acid glucoside.H^+, or $^{13}C_1$-iridoid-glucoside (e.g., harpagide).NH_4^+	5739	383.174725	2.07	10	7.27E−08
$^{13}C_2$-*O*-sulfoglucose.NH_4^+		5223	280.060038	7.54	16	4.22E−07
$^{13}C_2$-*O*-sulfoglucose.NH_4^+		7433	280.060048	7.54	17	5.57E−07
$^{13}C_6$-Hexose phosphate.H^+	(e.g., $^{13}C_6$-glucose 6-phosphate)	5157	267.056533	8.74	23	6.08E−06
$^{13}C_1$-Myoinositol phosphate-$H_2O.H^+$		7366	244.038910	7.53	26	1.13E−05
$^{13}C_6$-Hexose phosphate.H^+	(e.g., $^{13}C_6$-glucose 6-phosphate)	10833	267.056676	8.89	32	2.76E−05
$^{13}C_3$-Glucose.$Form_2$. $NH_3.Na^+$		9221	315.097173	7.55	34	3.02E−05
$^{13}C_3$-Gluconolactone 6-phosphate.NH_4^+		7431	279.056702	7.54	35	3.10E−05
$^{13}C_3$-Sucrose.H^+		8738	346.133719	3.33	43	5.62E−05
$^{13}C_{11}$-Sucrose.Na^+		5704	376.142859	4.25	49	8.07E-05
$^{13}C_3$-Sucrose.NH_4^+		2832	363.158327	4.45	58	1.70E−04
$^{13}C_6$-Hexose phosphate-$H_2O.H^+$	(e.g., $^{13}C_6$-glucose 6-phosphate)	9117	249.046237	8.54	60	1.83E−04
$^{13}C_1$-Sucrose.H^+		2639	344.126585	4.45	63	2.15E−04
$^{13}C_{11}$-Sucrose.NH_4+		5684	371.186311	4.67	71	3.11E−04
Nucleotides, bases and associated derivatives						
$^{13}C_3$-Adenosine monophosphate (K salt).Form-$3H_2O.NH_3.K^+$		5916	438.979622	2.44	4	9.45E−14
$^{13}C_2$-Methylhydroadenosine-H_2O.ACN.H^+		5400	309.158503	1.61	11	1.05E−07
$^{13}C_6$-UDP-glucose.NH_4^+		6139	590.109146	4.45	20	2.80E−06
$^{13}C_2$-Dehydrouridine-$NH_3.H^+$		5051	249.045988	4.67	30	2.55E−05
$^{13}C_2$-Dehydropyridine.H^+	(or its isomer $^{13}C_2$-aminopyrrole.H^+)	7102	85.067458	6.23	36	3.26E−05
$^{13}C_6$-UDP-glucose.NH_4^+		7749	590.107567	4.45	38	4.29E−05
$^{13}C_2$-Uracile.H^+		4431	115.048692	4.69	39	4.30E−05
$^{13}C_2$-Methyluridine.Na^+		5239	282.074027	4.69	44	5.66E−05
$^{13}C_1$,^{34}S-S-adenosyl homocysteinamine-$NH_3.H^+$		2470	329.125638	9.80	62	2.12E−04
Organic acids						
$^{13}C_2$-Gluconic acid.NH_4^+		4876	216.097253	2.53	5	2.18E−11

(Continues)

TABLE 1 (Continued)

Name	Possible identifications	Index MZMine	*m/z*	Retention time (min)	No.	*p* value
$^{13}C_2$-Glycolic acid-$H_2O.NH_4^+$		4340	78.046473	6.02	6	7.79E−11
$^{13}C_1$-Glycolic acid-$H_2O.NH_4^+$		4338	77.043133	6.04	8	7.20E−09
$^{13}C_2$-Citric acid.$(NH_3)_3$.HAc.Na^+		5492	328.132156	11.78	14	3.98E−07
$^{13}C_2$-*O*-feruloyl-malic acid.H^+		9220	313.086475	6.50	21	5.40E−06
$^{13}C_1$-Malic acid.NH_4^+		4566	153.057497	2.98	22	5.56E−06
$^{13}C_2$-Citric acid.$(NH_3)_3$.HAc.Na^+		8152	328.131636	11.78	25	8.56E−06
$^{13}C_2$-Citric acid.$(NH_3)_3$.HAc.Na^+		2456	328.131441	11.78	27	1.25E−05
$^{13}C_1$-Feruloyl-lactic acid.H^+		10855	284.083551	8.44	48	7.69E−05
Carboxyhydroxybenzoic acid.NH_4^+		947	200.055255	8.06	66	2.24E−04
Amino acids, peptides, polyamines and other derivatives						
$^{13}C_4$-Asparagine.H^+		4508	137.074118	7.65	12	1.92E−07
$^{13}C_1$-Methionine.H^+		517	151.060454	2.61	13	2.04E−07
$^{13}C_1$-Digalactosylcitrulline.H^+		6051	501.211734	3.20	15	4.09E−07
$^{13}C_1$-Tyr-Ser-Val peptide.NH_4^+		5750	386.210742	1.62	18	2.16E−06
$^{13}C_3$-Homoserine-$H_2O.H^+$		4399	105.056425	3.00	24	6.18E−06
$^{13}C_1$-Methionine-$NH_3.H^+$		4488	134.035115	2.98	28	1.42E−05
Phenylalanine.ACN.$H_3PO_4.NH_4^+$		8707	322.116116	2.58	31	2.56E−05
$^{13}C_1$-Methionine.H^+		518	151.061644	2.98	33	2.77E−05
$^{13}C_3$-Serine-$H_2O.H^+$		7108	91.049659	6.11	40	5.25E−05
$^{13}C_6$-Nicotinamide-$H_2O.H^+$		4422	111.064375	6.32	41	5.27E−05
$^{13}C_2$-*O*-acetylserine.H^+		512	150.064301	4.87	42	5.50E−05
O-sulfo-*N*-isoleucylproline.H^+		2246	309.111104	1.16	45	5.95E−05
$^{13}C_1$-Urea.H^+		7091	62.051678	6.21	47	7.64E−05
$^{13}C_3$-Serine.H^+		7124	109.060137	6.80	51	8.19E−05
$^{13}C_3$-Serine.H^+		4416	109.060168	6.01	54	1.13E−04
$^{13}C_2$-Serine.H^+		196	108.056013	6.96	56	1.29E−04
$^{13}C_2$-*O*-acetylserine.H^+		9468	150.063569	4.55	57	1.43E−04
$^{13}C_3$-Serine-$H_2O.H^+$		4368	91.049650	5.51	59	1.75E−04
$^{13}C_2$-*O*-sulfo-L-DOPA-H_2O.Form.H^+		5387	308.033676	6.04	61	1.86E−04
$^{13}C_6$-Cysteinylalanine-$NH_3.H^+$	(or its isomer $^{13}C_6$-Carbamoyl-methionine)	7226	182.057747	1.58	68	2.73E−04
$^{13}C_1$-Deamino *N*-formyl ornithine.Na^+		659	169.066188	2.07	70	2.81E−04
Secondary metabolites and unknowns						
Matairesinol.H^+		6823	359.148828	1.30	7	6.57E−10
$^{13}C_5$-Jasminoside S.NH_4^+		11998	515.270596	1.20	19	2.60E−06
$^{13}C_1$-Molecule*	$^{13}C_1$-Suberic acid.NH_4^+, or $^{13}C_1$-Proline betaine.Form.H^+, or $^{13}C_1$-*N*-lactoylvaline.H^+	4752	191.110963	2.37	29	2.36E−05
$^{13}C_1$-Molecule*	$^{13}C_1$-Octanoylcarnitine.H^+ or $^{13}C_1$-Isoprenoid (e.g., chrysanthemumine family).NH_4^+	1984	289.220101	3.29	37	4.25E−05
$^{13}C_1$-Quinic acid-$H_2O.NH_4^+$		875	193.090063	3.09	46	7.33E−05

TABLE 1 (Continued)

Name	Possible identifications	Index MZMine	*m/z*	Retention time (min)	No.	*p* value
$^{13}C_1$-Benzyl-glutathione.$(H^+)_2$		7268	200.577621	17.04	50	8.16E−05
Unknown		10363	65.823627	2.02	52	8.88E−05
$^{13}C_1$-Benzyl-glutathione.$(H^+)_2$		4795	200.577541	17.04	53	9.81E−05
Unknown		5501	330.128773	8.02	55	1.25E−04
$^{13}C_3$-Molecule*	$^{13}C_3$-Thr-Ser peptide.H^+, $^{13}C_3$-4-hydroxyaminopimelic acid.H^+, $^{13}C_3$-*O*-glycerylasparagine.H^+, $^{13}C_3$-*N*-acetylglutamic acid.NH_4^+, $^{13}C_3$-dehydroquinic acid-H_2O.NH_3.NH_4^+, or $^{13}C_3$-pyruvylthreonine.NH_4^+	4844	210.106663	4.46	64	2.21E−04
Peptide (several possibilities).H^+ or Glucosyl-xylitol.NH_4^+	*Possible peptides*: Ala-Gln-Asn, Gln-Gln-Gly, (Gly-Ala)2, Asn-(Ala)2-Gly, Gln-Asn-Ala	8722	332.152491	3.28	65	2.23E−04
$^{13}C_8$-Molecule*	$^{13}C_8$-Gln-Ala-Trp peptide.H^+ or $^{13}C_8$-glucosyl-methylsinapic alcohol.NH_4^+	5836	412.217973	1.77	67	2.64E−04
$^{13}C_6$-Molecule*	$^{13}C_6$-acetyldiglucosylgeraniol.NH_4^+, or $^{13}C_6$-acetyldiisovaleryl-sucrose.NH_4^+	6126	576.295285	1.73	69	2.79E−04

Note: The asterisk (*) indicates features the identity of which cannot be decided amongst possible compounds because their signal was too low to check the fragmentation pattern. In the sixth column, the number shown is the same as that used in Figure 3 and Supporting Information: Figure S4 (ordered by *p* value).

Abbreviations: ACN, acetonitrile; ANOVA, analysis of variance; Form, formic acid; HAc, acetic acid; LC-MS, liquid chromatography–mass spectrometry.

significantly higher during the chase (both dark and light) compared to that during the ^{13}C pulse. The relative ^{13}C-excess was more pronounced for $^{13}C_1$, $^{13}C_2$ and $^{13}C_6$ isotopologues. Since citrate derives from OAA, it would be of particular interest to look at the isotope pattern in OAA. However, OAA is an unstable metabolite present at low concentration. Rather, we looked at asparagine, which comes from OAA (via aspartate), contains four C-atoms, and was associated with an excellent signal (i.e., very good ionisation) in LC-MS (Figure 3c). It should be noted that asparagine is produced in sunflower mature leaves both in the light and in the dark, involving three isoforms of asparagine synthetase (Herrera-Rodríguez et al., 2004, 2007). The isotope pattern in asparagine was very different from that in citrate, with an increase in the $^{13}C_2$ isotopologue regardless of conditions (mole fraction of about 2%, while citrate $^{13}C_2$ isotopologue increased up to 4.3% under L conditions), and a disappearance of the $^{13}C_3$ and $^{13}C_4$ isotopologues during the chase in the light under $^{12}CO_2$. Unlike citrate, asparagine was thus mostly synthesised in the light with $^{13}CO_2$, and reciprocally, started to show isotopic dilution in the light with $^{12}CO_2$ (with relatively little impact on average molecular %^{13}C). However, like citrate, there was an increase in $^{13}C_1$ and $^{13}C_2$ isotopologues during the chase. These differences between citrate and asparagine can be reconciled considering the contribution of different carbon sources: a fumarate-malate pool (mostly unlabelled) and (phospho*enol*)pyruvate from triose phosphates (strongly labelled during the pulse), giving rise to partially labelled citrate and asparagine during the chase (Figure 3d).

Interestingly, two features with ^{13}C were associated with an increase in the light under $^{12}CO_2$ (chase) (Figure 3a): $^{13}C_5$-jasminoside S (β-citral glucoside) and $^{13}C_1$,^{34}S-S-adenosyl homocysteinamine. β-citral derives from carotenoid catabolism, thus suggesting that carotenoid turn-over did not use carbon from photosynthetic fixation and used 'old' carbon. S-adenosylhomocysteinamine is a derivative (demethylated and decarboxylated) of S-adenosylmethionine (SAM), generated in the source of the mass spectrometer. Its labelling under CO_2 at natural abundance shows that SAM turn-over (unrelated to methylation via tetrahydrofolate since the CH_3 group is not present in the LC-MS feature) did not coincide with photosynthesis but could use carbon fixed previously during the ^{13}C pulse.

Other metabolic pathways were highlighted by specific features, like arginine metabolism ($^{13}C_1$-deamino *N*-formyl ornithine, ^{13}C-urea, $^{13}C_1$-digalactosylcitrulline), phenylalanine derivatives ($^{12}C_2$-*O*-sulfo-L-DOPA, $^{13}C_2$-*O*-feruloyl-malate), oxidative pentose phosphate pathway (OPPP) ($^{13}C_3$-gluconolactone 6-phosphate, $^{13}C_2$-gluconate), isoleucine metabolism (*O*-sulfo-isoleucyl-proline) and adenylates ($^{13}C_3$-glyceryl-adenosine, $^{13}C_2$-methyl-hydroadenosine, $^{13}C_3$-adenosine monophosphate). The isotope pattern in selected features that may be associated with CO_2 production or utilisation was analysed (Supporting Information: Figure S6). The products of citrate metabolism, glutamate and glutamine, followed a similar pattern, with increased ^{13}C isotopologues during the chase. Amino acids (iso)leucine and tyrosine were also associated with a ^{13}C-enrichment during the pulse and then further ^{13}C-enrichment during the chase,

suggesting their metabolism was active both in the light and in the dark. The isotope pattern of phenylalanine (not shown) was identical to that of tyrosine. Adenine was ^{13}C-enriched regardless of conditions, with a prevalence of the $^{13}C_5$ isotopologue, showing that the ^{13}C-enrichment in adenylates was not only caused by their ribose moiety (i.e., general ^{13}C-enrichment in sugars) but also due to adenine turn-over itself.

4 | DISCUSSION

Untargeted analysis of metabolism during a ^{13}C pulse-chase experiment (with a total of 15 647 metabolic features per sample) was carried out to provide a broad picture of photosynthetic carbon utilisation in leaves, including by catabolism. In the discussion, we shall focus on potential links with leaf respiration, since several metabolic pathways revealed by isotopic labelling can produce or fix CO_2 (summarised in Figure 4). This aspect is of importance to better understand the metabolic origin of CO_2 evolved by respiration, the inhibition of leaf respiration by light, and highlight imperatives of respiratory metabolism in the light and in the dark (Tcherkez et al., 2017).

4.1 | Carbon utilisation during photosynthesis

Carbon fixed by photosynthesis was not only routed to sugars but also used to synthesise many compounds from various metabolic pathways, as revealed by either the decline in the monoisotopic species (^{12}C) or the increase in ^{13}C isotopologues (Figures 1–3). This included primary metabolites (amino acids, organic acids) but also secondary metabolites (phenylpropanoids) such as chlorogenate, which is a major compound in sunflowers (Abadie et al., 2018; Steck, 1968). It is interesting to note that phenylpropanoids are produced de novo from phenylalanine, which is synthesised in the chloroplast from erythrose 4-phosphate and PEP (Maeda & Dudareva, 2012). Since it is believed that there is no chloroplastic enolase (Voll et al., 2009), PEP must be synthesised in the cytosol and shuttled back to the chloroplast (Weber & Linka, 2011). The synthesis of phenylalanine derivatives also used stored carbon in particular in the dark, as suggested by the isotopic pattern, with an increase in the proportion of $^{13}C_3$ isotopologue, likely coming from the combination of $^{13}C_3$ PEP with ^{12}C-shikimate during chorismate synthesis (Supporting Information: Figure S6h). A similar dual origin of carbon to synthesise phenylalanine has been found previously (Abadie et al., 2018). Interestingly, a similar situation was observed here too

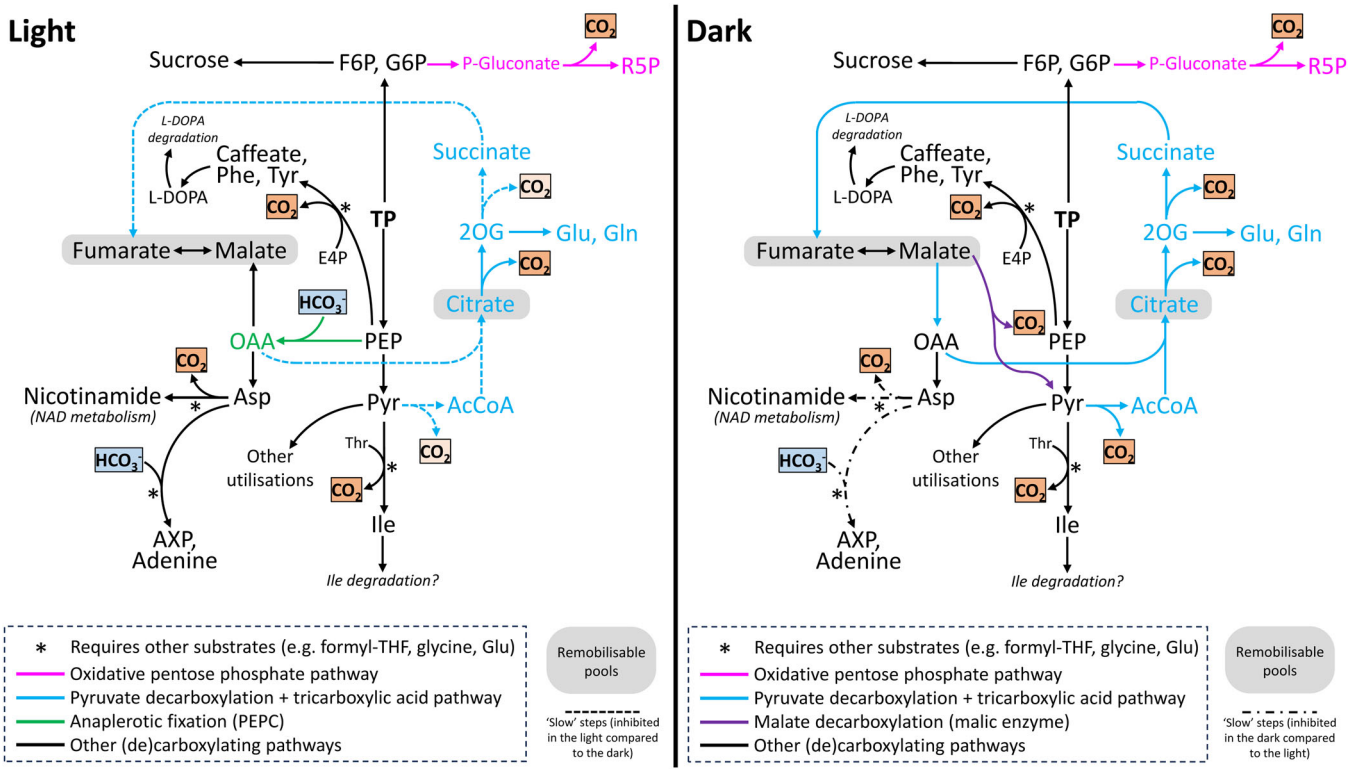

FIGURE 4 Summary of metabolic pathways associated with CO_2 production, as revealed by untargeted metabolomics. The specific involvement of PEP carboxylase and malic enzyme in light and dark, respectively, is shown to match fluxes found here (Table 2) and findings reported elsewhere. Fumarate and malate are considered collectively as a C_4 pool since they are interconvertible via fumarase. For simplicity, this figure does not include alternative pathways and thus only shows isoleucine production via threonine recycling, and NAD metabolism fed by aspartate rather than tryptophan. 'Other utilisations' include pyruvate consumption by, for example, lipid synthesis. 2OG, 2-oxoglutarate; AcCoA, acetyl-coenzyme A; AXP, adenylates; F6P, fructose 6-phosphate; G6P, glucose 6-phosphate; OAA, oxaloacetate; PEP, phospho*enol*pyruvate; Pyr, pyruvate; TP, triose phosphates. [Color figure can be viewed at wileyonlinelibrary.com]

with (iso)leucine, where the $^{13}C_2$ isotopologue prevailed, suggesting the use of $^{13}C_3$-pyruvate along with nonlabelled threonine (Supporting Information: Figure S6g).

Metabolic pathways associated with amino acids were both fed by carbon from current photosynthesis (and were thus ^{13}C-labelled) and turned over in the dark (thus with a decline in ^{13}C in the dark), that is, showing no strict light/dark cycle (Figure 3). This was typically the case with serine, (iso)leucine, arginine derivatives and asparagine. The dual carbon source for amino-acid and protein synthesis (current photosynthates, recycling) has been suggested before using near-natural ^{13}C abundance tracing (Schnyder et al., 2017). Amino-acid turnover has some potential to impact respiration since methionine and asparagine derive from aspartate (Galili, 2011), which in turn comes from OAA and thus from either the TCAP or PEPC activity. Also, de novo arginine synthesis requires carbamoyl phosphate synthesis (and thus CO_2 fixation) (Slocum, 2005), and (iso)leucine synthesis produces CO_2 (Binder et al., 2007). We note here that despite the apparent turnover of methionine in the dark, its ^{13}C abundance was mostly driven by its C-5 atom position (Supporting Information: Figure S5) and thus, by C-atom redistribution in C_1 metabolism rather than methionine synthesis from an unlabelled source, in agreement with the fact that methionine de novo synthesis occurs in the light (Hesse et al., 2004).

CO_2 (bicarbonate) was also fixed via PEPC, as demonstrated by (i) the production of $^{13}C_1$-malate (Figures 1 and 3a) and (ii) the appearance of $^{13}C_4$ isotopologues of asparagine in the light, with a pronounced ^{13}C atom excess (Figure 3c; see also scheme 2 in Figure 3d). Accordingly, malate was ^{13}C labelled during the pulse (much more than citrate, e.g.) and most of the ^{13}C-label disappeared during the chase in the light with $^{12}CO_2$ (Supporting Information: Figure S5).

4.2 | Citrate metabolism in the dark and in the light

Both NMR and LC-MS analysis pointed to citrate as a metabolite associated with a significant interaction effect. In fact, ^{13}C-labelled citrate was relatively low during the ^{13}C pulse in the light (not distinguishable from ^{13}C natural abundance using NMR) demonstrating that citrate synthesis from ^{13}C-precursors was minimal in the light. Conversely, citrate was ^{13}C-enriched during the chase, showing de novo synthesis of citrate took place in the dark (an estimate of citrate synthesis is provided in Supporting Information: Figure S7d). This direct piece of evidence via a pulse-chase is consistent with previous results obtained with a specific isotopic compound (with ^{13}C-pyruvate) fed to detached illuminated leaves (Tcherkez et al., 2005, 2008; Tcherkez, Mahe, et al., 2012). Here, it is also consistent with variation in citrate pool size, which was larger in darkness (Supporting Information: Figure S7c; Flis et al., 2019; Scheible et al., 2000), suggesting that it was partly consumed in the light.

Glutamate (and glutamine) production in the light consumed stored citrate or citrate synthesised de novo from stored ^{12}C-precursors. Using high-resolution NMR, calculations based on glutamate intramolecular ^{13}C distribution have suggested that about 70% of citrate consumed in the light was synthesised de novo (30% being consumed from the pre-existing citrate pool), 80% of which coming from stored precursors (Abadie, Lothier, et al., 2017). A similar conclusion has been reached using double ^{15}N-^{13}C labelling and spin-spin interaction monitoring in glutamate and glutamine (Gauthier et al., 2010). It means that in principle, only 14% of glutamate synthesised in the light during N assimilation consumes carbon from current photosynthesis. This is consistent with the isotopic pattern found here in glutamate, whereby the molecular %^{13}C was 4.5% in the light, much lower than the value found in the subsequent dark phase (17%, Supporting Information: Figure S6a). The nonlabelled carbon source used to synthesise citrate and glutamate in the light is likely made of (i) the malate + fumarate pool since malate interconverts with fumarate via fumarase, and fumarate was not visibly labelled (not shown) due to the enormous isotopic dilution by the considerable pool size in sunflower leaves (Abadie & Tcherkez, 2019a; Lawlor & Fock, 1977); (ii) pyruvate synthesised from malate via the malic enzyme and/or alanine transamination (i.e., pyruvate from alternative sources that would not be equilibrating with pyruvate from glycolysis). Here, we did not find alanine amongst the most significant features (although it was ^{13}C-labelled), suggesting that the alanine pool was mostly unlabelled (alanine %^{13}C was 12.9%, 9.9% and 2.7% under Light, Light + Dark and Light + Dark + Light conditions, respectively [data not shown] thus much less labelled than pyruvate, Supporting Information: Figure S5).

The use of stored carbon for citrate and glutamate synthesis in the light probably explains (i) why CO_2 produced by leaf day respiration is slow to capture ^{13}C (leading to $^{12}CO_2$ release in a $^{13}CO_2$ atmosphere and thus to isotopic disequilibrium (Gong et al., 2018)) and also (ii) the apparent disconnection (isotopic offset) between current photosynthates and day-respired CO_2 in gas exchange experiments at natural abundance where the $^{12}C/^{13}C$ isotope fractionation is measured (Barbour et al., 2017).

4.3 | Possible consequences for day and dark respiration

Our study provides an overview of major metabolic pathways that can have an influence on leaf respiration since ^{13}C labelling allowed us to identify turned-over metabolites. Of course, we recognise that our data cannot give access to metabolic pathways relying entirely on stored carbon (and thus not ^{13}C-labelled at all) or associated with products that were not analysed here (in particular lipids and nonwater-soluble secondary compounds). Despite this limitation, we took advantage of the isotopic enrichment found here in significant features to estimate (de) carboxylation fluxes and thus appreciate if we could reconstruct the metabolic origin of respired CO_2. That is, the change in ^{13}C content in metabolites and their precursors was used to calculate

the turnover of pools and thus the flux during each phase (Light, Light + Dark, Light + Dark + Light) of the experiment. Estimates are listed in Table 2 (along with a sensitivity analysis in Supporting Information: Figure S7a,b). This table does not show arginine metabolism since it was not possible to ascertain the metabolic pathway feeding the urea cycle and furthermore, arginine was not easily analysable by LC-MS under our chromatographic conditions. Taken as a whole, contributions of pathways other than the PEPC, TCAP (citrate utilisation) and malic enzyme were small, below 1 nmol m^{-2} s^{-1}. It was the case for the OPPP. However, its contribution was likely underestimated because its products (like free gluconate) have not been considered (free gluconate does not generate a good signal in LC-MS, impeding isotopologue analysis). A much larger contribution of cytosolic OPPP has been suggested (within 0.1–1 µmol m^{-2} s^{-1}, in particular at low light) using steady-state metabolic modelling (Buckley & Adams, 2011). Other studies have suggested significant OPPP activity in the light, playing the role of anaplerotic pentose phosphate provision when the photosynthetic demand is high, such as at high CO_2 (Sharkey, 2021; Wieloch et al., 2022; Xu et al., 2022). However, ^{14}C tracing has

TABLE 2 Estimation of CO_2 producing/consuming fluxes from present metabolic and isotopic data.

Metabolic process	µmol m^{-2} s^{-1}			Comments and limitations
	Light (Light, $^{13}CO_2$ pulse in the light)	Dark (Light + Dark, chase in darkness)	Light (Light + Dark + Light, chase in the light)	
CO_2 production				
(Iso)leucine metabolism	0.0008	0.066	*	Valine metabolism is not included here as valine isotopologues do not appear in significant features.
Phenylalanine metabolism	0.0003	0.007	*	Calculation based on phenylalanine turnover (since phenylalanine is the precursor of tyrosine and phenylpropanoids).
Malic enzyme activity	0	0.109	0	
Nicotinate metabolism (NAD synthesis)	0.0002	0.0003	*	
Glutamate production (PDH, I(C)DH)	0.235 (0.023;0.188)	0.689 (0.344;0.344)	0.136 (0.014;0.108)	Includes the dual contribution of stored citrate and de novo citrate synthesis.
Oxidative pentose phosphate pathway	<0.0001	0.0001	0.0001	Calculation based on gluconolactone turnover, so likely underestimates the flux since other compounds derived from phosphogluconate accumulate, such as free gluconate.
CO_2 consumption				
Phospho*enol*pyruvate carboxylase activity (anaplerotic fixation)	0.074	0	0.037	
Adenine synthesis	<0.0001	0.0001	0.0007	Uracile-derived nucleotides are not included in this table since uracile biosynthesis is CO_2-neutral.
Net flux (µmol m^{-2} s^{-1})	**0.209**	**1.56**	**0.125**	
Observed respiration rate (µmol m^{-2} s^{-1})	0.89 ± 0.36	1.83 ± 0.34	0.89 ± 0.36	R_d measured using the Laisk method in Abadie and Tcherkez (2019b).

Note: The bold is used to emphasize that it is the sum of values above. Reactions considered here are summarised in Figure 4. Arginine metabolism (urea production) is not considered in this table since the impact of urea synthesis in terms of CO_2 production depends on the original precursor (in particular if carbamoyl-phosphate is synthesised or not). Lysine metabolism is not considered here since it did not appear to be labelled under our conditions. See also Supporting Information: Table S3 for a more detailed presentation showing the estimated pool size and metabolic precursors used. The asterisk (*) indicates undefined flux (due to (i) an increase in $\%^{13}C$ in product and not in the precursor, suggesting some recycling [salvage pathway] or the contribution of another ^{13}C-labelled source; or (ii) lower than expected $\%^{13}C$ in product, suggesting the contribution of a nonlabelled source). By definition, this table cannot account for metabolic CO_2-producing pathways that were not followed in this study, for example, lipid synthesis and other nonsoluble compounds. For CO_2 associated with glutamate production, numbers between parentheses stand for CO_2 produced by PDH and I(C)DH, respectively (this does not represent total PDH and I(C)DH activities since acetyl-coenzyme A and 2-oxoglutarate can be used by pathways other than glutamate synthesis).

suggested chloroplastic OPPP is arrested in the light (Singh et al., 1993), and ^{13}C-glucose tracing has suggested minimal OPPP activity above 30 µmol m^{-2} s^{-1} light intensity in sunflower (Gauthier et al., 2020). Also, we recognise that in Table 2, other pathways associated with multiple branching points and several products could not be followed here or did not appear amongst significant features.

It should be kept in mind that a limitation of our calculations is that they do not consider compartmentalisation. In particular, organic acids like citrate, malate and fumarate can form separate pools in the vacuole and other cellular compartments and furthermore, the vacuole pool can be metabolically inactive or exhibit a very slow turn-over. For example, using nonaqueous fractionation of leaf tissues, malate has been found to be mostly distributed in the vacuole in spinach and *Arabidopsis* (Gerhardt & Heldt, 1984; Szecowka et al., 2013) while it was found to be nearly exclusively in the cytosol in another study in *Arabidopsis* (Krueger et al., 2011). Mathematically, it means that the effective %^{13}C in precursors used for calculations is probably different from (in practice, higher than) that of the total pool (i.e., isotopic dilution effect). A sensitivity analysis of CO_2 production associated with glutamate production from pyruvate and OAA as precursors shows that depending on the assumption made on %^{13}C in OAA or the contribution of stored carbon, the CO_2 efflux varies within 0.05 and 0.25 µmol m^{-2} s^{-1} (Supporting Information: Figure S7a,b), while standard parameterisation leads to a value of 0.23 µmol m^{-2} s^{-1} (conditions L; Table 2). However, our estimate in Table 2 is credible since in sunflower leaves, malate forms a comparatively small pool (same order of magnitude as glutamate, 2–5 mmol m^{-2}, more than five times less abundant than fumarate). Therefore, although being unavoidable in our analysis, the isotopic dilution effect on the malate/OAA active pool was probably modest.

Interestingly, the order of magnitude of dark respiration was satisfactory (1.5 µmol m^{-2} s^{-1}) showing that metabolomics-based reconstruction might be possible in darkness. In the light, net CO_2 efflux was considerably lower than observed day respiration (about 0.8 µmol m^{-2} s^{-1} in sunflower under the same conditions, estimated using the Laisk method), showing that CO_2-producing reactions that were nontraceable (due to entirely nonlabelled carbon sources) or missing from the present reconstruction using the metabolome. Still, fluxes associated with the TCAP and PEPC are consistent with other estimates provided elsewhere (Abadie & Tcherkez, 2019a; Tcherkez et al., 2008). Other fluxes not accounted for likely include pyruvate decarboxylation for lipid synthesis (≈0.1 µmol m^{-2} s^{-1}) and other biosyntheses (Tcherkez & Limami, 2019). In other words, our attempt to reconstruct CO_2 efflux strongly suggests that the diversity of CO_2 sources in observed day respiration is probably high in the light, that is, there are many CO_2-evolving metabolic pathways involved in day respiration, and they could not all be captured by our metabolomics-based analysis.

4.4 | Perspectives

Using untargeted, isotope-assisted metabolomics coupled with three techniques, we were able to look at metabolic pathways where metabolite turnover can impact on leaf respiration. As mentioned above, we recognise that this method does not give access to all CO_2-evolving reactions. In addition, classical methods used here focus on water-soluble compounds. Further studies will be necessary to extract and analyse nonsoluble compounds and thus appreciate more precisely the spectrum of pyruvate utilisation in the light. In fact, previous studies have shown that pyruvate decarboxylation and thus usage of acetyl-coenzyme A produced therefrom are much less inhibited in the light (compared to the dark) than TCAP activity (Tcherkez et al., 2005).

Also, although it represents a small flux, adenine turnover (which consumes CO_2) was observed in the light and the dark. We have previously shown that the ^{13}C enrichment in adenine depends on gaseous conditions (CO_2/O_2) (Abadie et al., 2021). In means that the adenylate pool is very dynamic and probably changes with photosynthetic and light conditions. Further studies are necessary to quantify precisely all adenylates and free adenine to appreciate the potential impact on ATP/ADP and photosynthesis itself. For example, it has been shown that perturbed purine biosynthesis (via the mutation of glutamine phosphoribosyl pyrophosphate amidotransferase 2) impacts the photosynthetic machinery and acclimation to high light (Woo et al., 2011). Similarly, our present data show that uridylate metabolism is very dynamic, with a visible turnover of uracile and uridine. While this should not impact directly on CO_2 efflux, the potential photosynthetic control of UTP, UDP and UDP-glucose content via the regulation of uracile biosynthesis would deserve further attention.

ACKNOWLEDGEMENTS

The authors would like to thank the Joint Mass Spectrometry Facility at the Australian National University (ANU) for allowing access to instruments. They would also like to thank the financial support of the Région Pays de la Loire and Angers Loire Métropole via the grant Connect Talent Isoseed. Open access publishing facilitated by Australian National University, as part of the Wiley - Australian National University agreement via the Council of Australian University Librarians.

CONFLICT OF INTEREST STATEMENT

The authors declare no conflict of interest.

DATA AVAILABILITY STATEMENT

Numerical data are provided in this manuscript. Original raw data are provided as a supplemental Excel file.

ORCID

Anis M. Limami http://orcid.org/0000-0002-9985-2363
Guillaume Tcherkez http://orcid.org/0000-0002-3339-956X

REFERENCES

Abadie, C., Bathellier, C. & Tcherkez, G. (2018) Carbon allocation to major metabolites in illuminated leaves is not just proportional to photosynthesis when gaseous conditions (CO_2 and O_2) vary. *New Phytologist*, 218, 94–106.

Abadie, C., Blanchet, S., Carroll, A. & Tcherkez, G. (2017) Metabolomics analysis of post-photosynthetic effects of gaseous O_2 on primary metabolism in illuminated leaves. *Functional Plant Biology*, 44, 929–940.

Abadie, C., Lalande, J., Limami, A.M. & Tcherkez, G. (2021) Non-targeted ^{13}C metabolite analysis demonstrates broad re-orchestration of leaf metabolism when gas exchange conditions vary. *Plant, Cell & Environment*, 44, 445–457.

Abadie, C., Lothier, J., Boex-Fontvieille, E., Carroll, A. & Tcherkez, G. (2017) Direct assessment of the metabolic origin of carbon atoms in glutamate from illuminated leaves using ^{13}C-NMR. *New Phytologist*, 216, 1079–1089.

Abadie, C. & Tcherkez, G. (2019a) In vivo phosphoenolpyruvate carboxylase activity is controlled by CO_2 and O_2 mole fractions and represents a major flux at high photorespiration rates. *New Phytologist*, 221, 1843–1852.

Abadie, C. & Tcherkez, G. (2019b) Plant sulphur metabolism is stimulated by photorespiration. *Nature Communications Biology*, 2, 1–7.

Araújo, W.L., Nunes-Nesi, A., Nikoloski, Z., Sweetlove, L.J. & Fernie, A.R. (2012) Metabolic control and regulation of the tricarboxylic acid cycle in photosynthetic and heterotrophic plant tissues. *Plant, Cell & Environment*, 35, 1–21.

Araújo, W.L., Nunes-Nesi, A., Trenkamp, S., Bunik, V.I. & Fernie, A.R. (2008) Inhibition of 2-oxoglutarate dehydrogenase in potato tuber suggests the enzyme is limiting for respiration and confirms its importance in nitrogen assimilation. *Plant Physiology*, 148, 1782–1796.

Atkin, O.K., Bahar, N.H.A., Bloomfield, K.J., Griffin, K.L., Heskel, M.A. Huntingford, C. et al. (2017) Leaf respiration in terrestrial biosphere models. In: Tcherkez, G. & Ghashghaie, J. (Eds.) *Plant respiration: metabolic fluxes and carbon balance*. Berlin: Springer, pp. 107–142.

Atkin, O.K., Bloomfield, K.J., Reich, P.B., Tjoelker, M.G., Asner, G.P., Bonal, D. et al. (2015) Global variability in leaf respiration in relation to climate, plant functional types and leaf traits. *New Phytologist*, 206, 614–636.

Atkin, O.K., Meir, P. & Turnbull, M.H. (2014) Improving representation of leaf respiration in large-scale predictive climate-vegetation models. *New Phytologist*, 202, 743–748.

Atkin, O.K., Westbeek, M., Cambridge, M.L., Lambers, H. & Pons, T.L. (1997) Leaf respiration in light and darkness (a comparison of slow- and fast-growing *Poa* species). *Plant Physiology*, 113, 961–965.

Aubert, S., Gout, E., Bligny, R. & Douce, R. (1994) Multiple effects of glycerol on plant cell metabolism. Phosphorus-31 nuclear magnetic resonance studies. *Journal of Biological Chemistry*, 269, 21420–21427.

Bacher, A., Chen, F. & Eisenreich, W. (2016) Decoding biosynthetic pathways in plants by pulse-chase strategies using $^{13}CO_2$ as a universal tracer. *Metabolites*, 6, Article no 21.

Barbour, M.M., Ryazanova, S. & Tcherkez, G. (2017) Respiratory effects on carbon isotope discrimination near the compensation point. In: Tcherkez, G. & Ghashghaie, J., (Eds). *Plant Respiration: Metabolic Fluxes and Carbon Balance. In Advances in Photosynthesis and Respiration*. Berlin: Springer Netherlands. pp. 143–160.

Binder, S., Knill, T. & Schuster, J. (2007) Branched-chain amino acid metabolism in higher plants. *Physiologia Plantarum*, 129, 68–78.

Buckley, T.N. & Adams, M.A. (2011) An analytical model of non-photorespiratory CO_2release in the light and dark in leaves of C_3 species based on stoichiometric flux balance. *Plant, Cell & Environment*, 34, 89–112.

Budde, R.J. & Randall, D.D. (1990) Pea leaf mitochondrial pyruvate dehydrogenase complex is inactivated in vivo in a light-dependent manner. *Proceedings of the National Academy of Sciences of the United States of America*, 87, 673–676.

Bylesjö, M., Rantalainen, M., Cloarec, O., Nicholson, J.K., Holmes, E. & Trygg, J. (2006) OPLS discriminant analysis: combining the strengths of PLS-DA and SIMCA classification. *Journal of Chemometrics*, 20, 341–351.

Dieuaide-Noubhani, M., Alonso, A.-P., Rolin, D., Eisenreich, W. & Raymond, P. (2007) Metabolic flux analysis: Recent advances in carbon metabolism in plants. In: Baginsky, S. & Fernie, A.R., (Eds.) *Plant Systems Biology*. Basel: Birkhäuser Basel. pp. 213–243.

Eriksson, L., Trygg, J. & Wold, S. (2008) CV-ANOVA for significance testing of PLS and OPLS® models. *Journal of Chemometrics*, 22, 594–600.

Farquhar, G.D., Ehleringer, J.R. & Hubick, K.T. (1989) Carbon isotope discrimination and photosynthesis. *Annual Review of Plant Physiology and Plant Molecular Biology*, 40, 503–537.

Flis, A., Mengin, V., Ivakov, A.A., Mugford, S.T., Hubberten, H.-M., Encke, B. et al. (2019) Multiple circadian clock outputs regulate diel turnover of carbon and nitrogen reserves. *Plant, Cell & Environment*, 42, 549–573.

Galili, G. (2011) The aspartate-family pathway of plants: linking production of essential amino acids with energy and stress regulation. *Plant Signaling & Behavior*, 6, 192–195.

Gauthier, P.P.G., Bligny, R., Gout, E., Mahé, A., Nogués, S., Hodges, M. et al. (2010) In folio isotopic tracing demonstrates that nitrogen assimilation into glutamate is mostly independent from current CO_2 assimilation in illuminated leaves of *Brassica napus*. *New Phytologist*, 185, 988–999.

Gauthier, P.P.G., Saenz, N., Griffin, K.L., Way, D. & Tcherkez, G. (2020) Is the Kok effect a respiratory phenomenon? Metabolic insight using ^{13}C labeling in *Helianthus annuus* leaves. *New Phytologist*, 228, 1243–1255.

Gemel, J. & Randall, D.D. (1992) Light regulation of leaf mitochondrial pyruvate dehydrogenase complex: role of photorespiratory carbon metabolism. *Plant Physiology*, 100, 908–914.

Gerhardt, R. & Heldt, H.W. (1984) Measurement of subcellular metabolite levels in leaves by fractionation of freeze-stopped material in nonaqueous media. *Plant Physiology*, 75, 542–547.

Gessler, A., Roy, J., Kayler, Z., Ferrio, J.P., Alday, J.G., Bahn, M. et al. (2017) Night and day-circadian regulation of night-time dark respiration and light-enhanced dark respiration in plant leaves and canopies. *Environmental and Experimental Botany*, 137, 14–25.

Gong, X.Y., Schäufele, R., Lehmeier, C.A., Tcherkez, G. & Schnyder, H. (2017) Atmospheric CO_2 mole fraction affects stand-scale carbon use efficiency of sunflower by stimulating respiration in light. *Plant, Cell & Environment*, 40, 401–412.

Gong, X.Y., Tcherkez, G., Wenig, J., Schäufele, R. & Schnyder, H. (2018) Determination of leaf respiration in the light: comparison between an isotopic disequilibrium method and the Laisk method. *New Phytologist*, 218, 1371–1382.

Gout, E., Bligny, R., Pascal, N. & Douce, R. (1993) ^{13}C nuclear magnetic resonance studies of malate and citrate synthesis and compartmentation in higher plant cells. *Journal of Biological Chemistry*, 268, 3986–3992.

Graham, D. & Walker, D. (1962) Some effects of light on the interconversion of metabolites in green leaves. *Biochemical Journal*, 82, 554–560.

Hanning, I. & Heldt, H.W. (1993) On the function of mitochondrial metabolism during photosynthesis in spinach (*Spinacia oleracea* L.) leaves (partitioning between respiration and export of redox equivalents and precursors for nitrate assimilation products). *Plant Physiology*, 103, 1147–1154.

Herrera-Rodríguez, M.B., Maldonado, J.M. & Pérez-Vicente, R. (2004) Light and metabolic regulation of HAS1, HAS1.1 and HAS2, three asparagine synthetase genes in *Helianthus annuus*. *Plant Physiology and Biochemistry*, 42, 511–518.

Herrera-Rodríguez, M.B., Pérez-Vicente, R. & Maldonado, J.-M. (2007) Expression of asparagine synthetase genes in sunflower (*Helianthus annuus*) under various environmental stresses. *Plant Physiology and Biochemistry*, 45, 33–38.

Heskel, M.A., Atkin, O.K., Turnbull, M.H. & Griffin, K.L. (2013) Bringing the Kok effect to light: A review on the integration of daytime respiration and net ecosystem exchange. *Ecosphere*, 4, 1–14.

Hesse, H. (2004) Current understanding of the regulation of methionine biosynthesis in plants. *Journal of Experimental Botany*, 55, 1799–1808.

Huege, J., Sulpice, R., Gibon, Y., Lisec, J., Koehl, K. & Kopka, J. (2007) GC-EI-TOF-MS analysis of in vivo carbon-partitioning into soluble metabolite pools of higher plants by monitoring isotope dilution after ^{13}CO2 labelling. *Phytochemistry*, 68, 2258–2272.

Huntingford, C., Atkin, O.K., Martinez-de la Torre, A., Mercado, L.M., Heskel, M.A., Harper, A.B. et al. (2017) Implications of improved representations of plant respiration in a changing climate. *Nature Communications*, 8, Article no 1602.

Krueger, S., Giavalisco, P., Krall, L., Steinhauser, M.-C., Büssis, D., Usadel, B. et al. (2011) A topological map of the compartmentalized *Arabidopsis thaliana* leaf metabolome. *PloS one*, 6, Article no e17806.

Laisk, A. & Loreto, F. (1996) Determining photosynthetic parameters from leaf CO_2 exchange and chlorophyll fluorescence (ribulose-1, 5-bisphosphate carboxylase/oxygenase specificity factor, dark respiration in the light, excitation distribution between photosystems, alternative electron transport rate, and mesophyll diffusion resistance. *Plant Physiology*, 110, 903–912.

Lawlor, D.W. & Fock, H. (1977) Water stress induced changes in the amounts of some photosynthetic assimilation products and respiratory metabolites of sunflower leaves. *Journal of Experimental Botany*, 28, 329–337.

Maeda, H. & Dudareva, N. (2012) The shikimate pathway and aromatic amino acid biosynthesis in plants. *Annual Review of Plant Biology*, 63, 73–105.

O'Leary, B.M., Asao, S., Millar, A.H. & Atkin, O.K. (2019) Core principles which explain variation in respiration across biological scales. *New Phytologist*, 222, 670–686.

Scheible, W.R., Krapp, A. & Stitt, M. (2000) Reciprocal diurnal changes of phospho*enol*pyruvate carboxylase expression and cytosolic pyruvate kinase, citrate synthase and NADP-isocitrate dehydrogenase expression regulate organic acid metabolism during nitrate assimilation in tobacco leaves. *Plant, Cell & Environment*, 23, 1155–1167.

Schnyder, H., Ostler, U. & Lehmeier, C.A. (2017) Respiratory turn-over and metabolic compartments: from the design of tracer experiments to the characterization of respiratory substrate-supply systems. In: Tcherkez, G. & Ghashghaie, J. (Eds.) *Plant respiration: metabolic fluxes and carbon balance*. Cham: Springer International Publishing, pp. 161–179.

Schnyder, H., Ostler, U., Lehmeier, C., Wild, M., Morvan-Bertrand, A. & Schäufele, R. et al. (2012) Tracing carbon fluxes: resolving complexity using isotopes. In: Matyssek, R., Schnyder, H., Oßwald, W., Ernst, D., Munch, J. & Pretzsch, H. (Eds.) *Growth and defence in plants: resource allocation at multiple scales*. Berlin: Springer, pp. 157–173.

Sharkey, T.D. (2021) Pentose phosphate pathway reactions in photosynthesizing cells. *Cells*, 10, 1547. Available from: https://doi.org/10.3390/cells10061547

Singh, K.K., Chen, C. & Gibbs, M. (1993) Photoregulation of fructose and glucose respiration in the intact chloroplasts of *Chlamydomonas reinhardtii* F-60 and spinach. *Plant Physiology*, 101, 1289–1294.

Slocum, R.D. (2005) Genes, enzymes and regulation of arginine biosynthesis in plants. *Plant Physiology and Biochemistry*, 43, 729–745.

Steck, W. (1968) Metabolism of cinnamic acid in plants: chlorogenic acid formation. *Phytochemistry*, 7, 1711–1717.

Szecowka, M., Heise, R., Tohge, T., Nunes-Nesi, A., Vosloh, D., Huege, J. et al. (2013) Metabolic fluxes in an illuminated *Arabidopsis* rosette. *The Plant Cell*, 25, 694–714.

Tan, Y.D. & Xu, H. (2014) A general method for accurate estimation of false discovery rates in identification of differentially expressed genes. *Bioinformatics*, 30, 2018–2025.

Tcherkez, G., Bligny, R., Gout, E., Mahé, A., Hodges, M. & Cornic, G. (2008) Respiratory metabolism of illuminated leaves depends on CO_2 and O_2 conditions. *Proceedings of the National Academy of Sciences of the United States of America*, 105, 797–802.

Tcherkez, G., Boex-Fontvieille, E., Mahé, A. & Hodges, M. (2012) Respiratory carbon fluxes in leaves. *Current Opinion in Plant Biology*, 15, 308–314.

Tcherkez, G., Cornic, G., Bligny, R., Gout, E. & Ghashghaie, J. (2005) In vivo respiratory metabolism of illuminated leaves. *Plant Physiology*, 138, 1596–1606.

Tcherkez, G., Gauthier, P., Buckley, T.N., Busch, F.A., Barbour, M.M., Bruhn, D. et al. (2017) Leaf day respiration: low CO_2 flux but high significance for metabolism and carbon balance. *New Phytologist*, 216, 986–1001.

Tcherkez, G. & Limami, A.M. (2019) Net photosynthetic CO_2 assimilation: more than just CO_2 and O_2 reduction cycles. *New Phytologist*, 223, 520–529.

Tcherkez, G., Mahé, A., Gauthier, P., Mauve, C., Gout, E., Bligny, R. et al. (2009) In folio respiratory fluxomics revealed by ^{13}C isotopic labeling and H/D isotope effects highlight the noncyclic nature of the tricarboxylic acid "cycle" in illuminated leaves. *Plant Physiology*, 151, 620–630.

Tcherkez, G., Mahe, A., Guerard, F., Boex-Fontvieille, E.R.A., Gout, E., Lamothe, M. et al. (2012b) Short-term effects of CO_2 and O_2 on citrate metabolism in illuminated leaves. *Plant, Cell and Environment*, 35, 2208–2220.

Tcherkez, G., Mauve, C., Lamothe, M., Le Bras, C. & Grapin, A. (2011) The $^{13}C/^{12}C$ isotopic signal of day-respired CO_2 in variegated leaves of *Pelargonium × hortorum*. *Plant, cell & environment*, 34, 270–283.

Versluys, M., Kirtel, O., Toksoy Öner, E. & Van den Ende, W. (2018) The fructan syndrome: evolutionary aspects and common themes among plants and microbes. *Plant, Cell & Environment*, 41, 16–38.

Voll, L.M., Hajirezaei, M.R., Czogalla-Peter, C., Lein, W., Stitt, M., Sonnewald, U. et al. (2009) Antisense inhibition of enolase strongly limits the metabolism of aromatic amino acids, but has only minor effects on respiration in leaves of transgenic tobacco plants. *New Phytologist*, 184, 607–618.

Weber, A.P.M. & Linka, N. (2011) Connecting the plastid: transporters of the plastid envelope and their role in linking plastidial with cytosolic metabolism. *Annual Review of Plant Biology*, 62, 53–77.

Wieloch, T., Augusti, A. & Schleucher, J. (2022) Anaplerotic flux into the Calvin–Benson cycle: hydrogen isotope evidence for in vivo occurrence in C_3 metabolism. *New Phytologist*, 234, 405–411.

Wingate, L., Seibt, U., Moncrieff, J.B., Jarvis, P.G. & Lloyd, J. (2007) Variations in ^{13}C discrimination during CO_2 exchange by *Picea sitchensis* branches in the field. *Plant, Cell & Environment*, 30, 600–616.

Woo, N.S., Gordon, M.J., Graham, S.R., Rossel, J.B., Badger, M.R. & Pogson, B.J. (2011) A mutation in the purine biosynthetic enzyme ATASE2 impacts high light signalling and acclimation responses in green and chlorotic sectors of *Arabidopsis* leaves. *Functional Plant Biology*, 38, 401–419.

Xu, Y., Wieloch, T., Kaste, J.A.M., Shachar-Hill, Y. & Sharkey, T.D. (2022) Reimport of carbon from cytosolic and vacuolar sugar pools into the

Calvin–Benson cycle explains photosynthesis labeling anomalies. *Proceedings of the National Academy of Sciences of the United States of America*, 119, e2121531119.

SUPPORTING INFORMATION

Additional supporting information can be found online in the Supporting Information section at the end of this article.

How to cite this article: Abadie, C., Lalande, J., Dourmap, C., Limami, A.M. & Tcherkez, G. (2024) Leaf day respiration involves multiple carbon sources and depends on previous dark metabolism. *Plant, Cell & Environment*, 47, 2146–2162. https://doi.org/10.1111/pce.14871